Pulsed NMR: Relaxation times as function of viscocity and impurities

Tony Hyun Kim
MIT Department of Physics
(Dated: November 18, 2008)

We measure the spin-lattice (T_1) and spin-spin (T_2) relaxation times of a sample of nuclear spins, as a function of viscosity and impurity concentration. In the viscosity study, we confirm Bloembergen's observation of an inverse-law relationship between relaxation times and viscosity. The impurity investigation remains inconclusive. In general, our measurements support the claim that microscopic complexity (increased viscosity; additional impurities) increases relaxation rates.

1. INTRODUCTION

Modern attempts to utilize quantum mechanics for novel applications (e.g. quantum computing) are severely limited by the *relaxation times* associated with the particular implementation. Relaxation times describe the timescale for which the system remains under coherent control by the experimenter. In this paper, we investigate the dynamics of an ensemble of nuclear spins as a prototype for the relaxation phenomenon.

We manipulate a sample of nuclear spins by the techniques of nuclear magnetic resonance (NMR) developed by Felix Bloch and E.M. Purcell, through which the spin ensemble can be perturbed away from thermal equilibrium. Following the excitation, we observe an exponential decay in the fraction of the sample following coherent evolution, which is the relaxation effect. We have measured relaxation along two dimensions: the *spin-lattice* relaxation time (T_1) which describes the return to thermal occupation of the eigenstates; and the *spin-spin* relaxation time (T_2) which is the disappearance of the coherent evolution due to "dephasing" among the individual spins. In an upcoming section, we will explain more explicitly the two effects in the context of a spin system.

We have considered the relaxation times T_1, T_2 as a function of viscosity of the sample, and as a function of magnetic impurity concentration. In both cases, we observe that relaxation times are shortened (more rapid decay) when additional interactions are added (i.e. more viscous; additional impurities). In the viscosity study, we have verified Bloembergen's observation of an inverse-law relationship.[1]

2. THEORETICAL BACKGROUND

2.1. Coherent manipulation of nuclear spins

NMR experiments are conducted in a region of large bias field B_0. In our experiment, the nuclear spin is that of the proton ^1H in glycerine and water molecules. Because ^1H has total nuclear spin $I = 1/2$[2], there are two possibilities for the spin projection: $|+\rangle$ (aligned with B_0) and $|-\rangle$ (anti-aligned). In thermal equilibrium, the sample occupies the eigenstates $|+\rangle$ and $|-\rangle$ in accordance with the Boltzmann distribution.

The system is then perturbed by a small oscillating magnetic field $B_1 = B_{1,0}\cos(\omega t)$ in a direction perpendicular to the bias field B_0. The interaction between the applied field $\vec{B} = \vec{B_0} + \vec{B_1}$ and the nuclear spin is due to the magnetic Hamiltonian $H = -\vec{\mu}\cdot\vec{B}$, where $\vec{\mu} = \gamma\vec{I}$ is the magnetic moment associated with the spin, and γ is the gyromagnetic ratio. In a static B-field, the (expectation of the) magnetic moment undergoes precessive motion about B at the Larmor frequency $w_L = \gamma B_0$. The experimental signature of such collective precession is RF radiation, which is the basic detection mechanism in our experiment. The observed oscillatory response is called the *free induction decay* (FID). The dynamics is more complicated for a time-dependent B. We give only a cursory analysis for the time-dependent case; a detailed and geometrically-enlightening discussion can be found in [3, 4].

For our time-dependent field $\vec{B}(t) = B_1(t)\vec{e}_x + B_0\vec{e}_z$, we represent the spinor $|\psi\rangle$ in the basis of the static field eigenstates $\{|+\rangle, |-\rangle\}$ as in:

$$|\psi(t)\rangle = \begin{bmatrix} C_u(t)e^{+i\frac{\omega_L}{2}t} \\ C_d(t)e^{-i\frac{\omega_L}{2}t} \end{bmatrix} \tag{1}$$

where the exponential factor corresponds to the standard time-evolution due to the bias field B_0. (The splitting between $|+\rangle$ and $|-\rangle$ corresponds to the Larmor frequency.) It can be shown[4] that the Schrödinger equation in the above basis yields:

$$\dot{C}_u = \frac{i\omega_x}{2}C_d\left[e^{i(\omega-\omega_L)t} + e^{-i(\omega+\omega_L)t}\right] \tag{2}$$

$$\dot{C}_d = -\frac{i\omega_x}{2}C_u\left[e^{i(\omega-\omega_L)t} + e^{-i(\omega+\omega_L)t}\right] \tag{3}$$

with $\omega_x = \mu B_{1,0}/\hbar$. Now, on *resonance* ($\omega = \omega_L$) the above equations reduce to a set of coupled harmonic oscillators in C_u and C_d. (We take the time average of the rapid oscillation $\langle e^{-i2\omega_L t}\rangle = 0$.) In other words, during the interval for which a resonant transverse field B_1 is applied, the spinor undergoes *Rabi oscillations* between the two static eigenstates. By properly timing the duration of the B_1 "pulse", it is possible to invert the spin state (the so-called "180° pulse"; i.e. $|+\rangle \rightarrow |-\rangle$ and vice versa), or even drive the spinor to a superposition state whose expectation lies in the transverse plane (a "90° pulse"). In principle, such a vector remains in the superposition state indefinitely.

2.2. Spin-lattice relaxation, T_1

In the actual experiment, however, the samples are free to exchange energy with the environment (the "lattice"). Therefore, the superposition state is energetically permitted to undergo wavefunction collapse into one of the eigenstates, thereby losing the component undergoing precession. The timescale of the return to the bias field axis is called the spin-lattice relaxation time T_1.

We have chosen to measure T_1 by using a $90° - \tau - 90°$ pulse sequence. In this experiment, we first drive the spins into the transverse plane using a 90° pulse. We then wait a period τ, during which some of the precessing spins will have collapsed into the eigenstates. By applying a second 90° pulse, we then bring the collapsed spins back into precession. At the same time, the second pulse sends the initially uncollapsed spins towards the bias field axis. By considering the size of the secondary FID, we can deduce the timescale of the spin-lattice relaxation.

2.3. Spin-spin relaxation, T_2

Even when the spin ensemble does not interact with the surroundings, the internal interaction among the spins can result in *decoherence* of the precessive motion. As we have remarked earlier, the macroscopic Hamiltonian due to the static B_0-field should in principle result in perpetual precession. However, the actual Hamiltonian experienced by the spins includes microscopic effects such as the μ/r^3 spin-spin interactions among the nuclei. Furthermore, the bias field inhomogeneity and diffusion of individual spins through the volume all contribute as to yield a complicated microscopic Hamiltonian that is inconsistent with the coherent, precessive motion of the macroscopic Hamiltonian.

Thus there is potential for loss of transverse magnetization without collapse into the eigenstates. This is known as the spin-spin relaxation T_2. Among the above effects, the most fundamental is the spin-spin interaction, since the other effects are not intrinsic to the system. Moreover, there exist experimental procedures for overcoming the latter effects, as we now show.

Consider a purely non-diffusive sample in an inhomogeneous bias field. We can partition the sample into sufficiently small regions for which the local field is well-approximated to be uniform. In such a partition, each region has a fixed frequency of precession. Note that even in the case of ideal, non-interacting spins, the overall transverse magnetization will then be seen to decay, because the spins of different regions will evolve out of phase. In 1950, E. Hahn showed that a 180° pulse to such a system will precisely reverse the relative phase accumulation in the different regions, so that the in-phase dynamics is recovered (the "spin echo") at some time following the 180° pulse.[5] (See Fig. 1.)

We measure T_2 by the Carr-Purcell (CP) pulse sequence, consisting of the following pulses: $90° - \tau - 180° - 2\tau - 180° - 2\tau - ...$, where τ is a fixed waiting period. The ensemble responds to the CP sequence with a spin-echo halfway between each 180° pulses. By choosing a small τ, we can even diminish the effect of diffusion in the sample, since there will be little time for the spins to move in between pulses. By considering the decay of the echo heights, we then calculate the loss of transverse magnetization in a way independent of the bias field inhomogeneity and diffusion effects.

3. EXPERIMENTAL SETUP

The experimental apparatus consisted of a $B_0 = 1770$ gauss permanent magnet, RF drive and detection circuit, and a PC-based oscilloscope-capture card as shown in Figure 1.

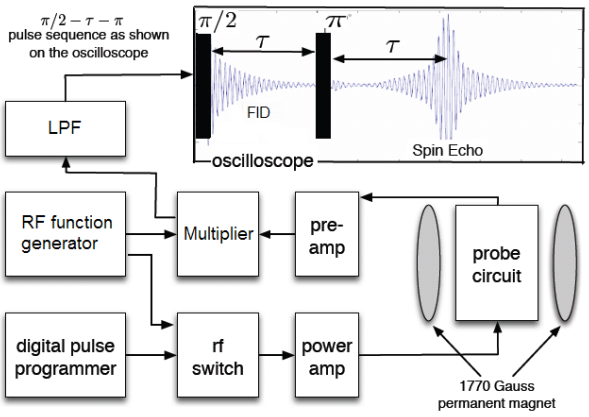

FIG. 1: Schematic of the experimental apparatus. The scope trace shows the spin echo that arises due to a 180° pulse following the decay of the initial FID. Figure from [6]

The function generator provided a continuous sinusoid, yielding a RF drive of approximately 25V(pp) at the probe. We generated pulses of desired duration by gating this signal with a switch, using logic from a digital pulse programmer. A major shortcoming of the apparatus was the limited precision with which we could time the pulses. In particular, we had a timing resolution of 1μs, which was not sufficient for the generation of 180° pulses (and by implication also the 90° pulses). When a 180° pulse is applied to the thermal sample, we do not expect any FID. However, during the experiment, we found that it was impossible to adjust the parameters as to give a 180° pulse that did not produce some FID.

The gated RF signal was amplified and sent to the probe circuit, consisting of a solenoid wrapped around a vial containing the NMR sample. During the readout step of the experiment, the same solenoid was used to detect the precessing spins by magnetic induction.

The multiplier and the LPF allowed us to quantitatively estimate the resonant frequency of the samples. In general, the applied frequency ω and the spin precession

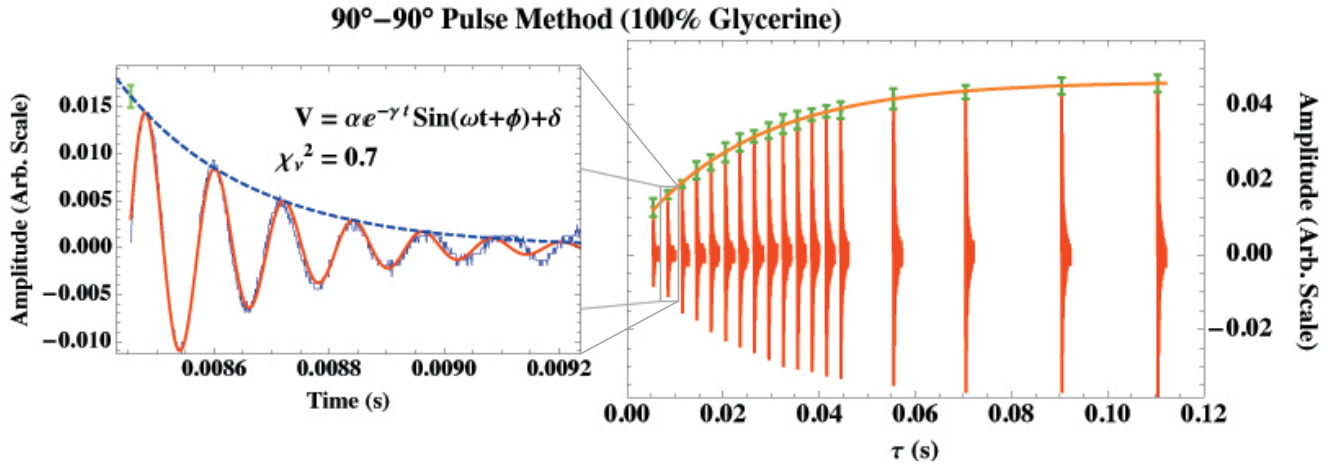

FIG. 2: The $90° - \tau - 90°$ pulse method applied to a sample of 100% glycerine. (Left) A single FID fit against $V(t) = \alpha e^{-\gamma t}\sin(\omega t + \phi) + \delta$. The decaying envelope is plotted and the extrapolated amplitude is placed with its corresponding error bar. (Right) FIDs of various τ are superimposed, and an exponential envelope is fitted. From this regression, it is found that $T_1 = 25.0 \pm 0.6$ ms.

rate ω_L will not be identical. Recall that the effect of a multiplier is to produce a superposition of two sinusoids at the difference and sum frequencies. The LPF preserves only the difference frequency. Hence, the apparatus offered an observable benchmark for being "on-resonance": at resonance, we observed a severely band-limited signal on the oscilloscope. We were also able to obtain an error in our estimate of ω_L by examining the frequency content of the final signal via a Fourier transform.

For the remainder of the experiment, the multiplier/LPF chain was a slight detriment, because we were forced to purposely move off of resonance (order of kHz), in order to observe reasonable FIDs. Since our pulse durations were around 50μs, this slightly invalidates our assumption of perfect Rabi oscillations over the pulse duration, i.e. that $e^{i(\omega-2\omega_0)t} = 1$ over the interval.

Finally, a major limitation in our experiment was the rather slow sampling rate ($T_{sample} = 25\mu$s for the T_2 measurements) of the oscilloscope acquisition. In some of our runs, we have noticed significant discrepancies on the actual oscilloscope trace, and the PC-acquired data. This is troublesome for our estimates for the heights of peaks, since the actual maximum of a peak may have been aliased in the sampling process. We also note that the acquisition software converted the signal into arbitrary units; and that it introduced quantization errors of 0.6×10^{-3} in the arbitrary units.

4. RESULTS AND DISCUSSION

4.1. Determination of resonant frequencies and the gyromagnetic ratio

We have performed ten measurements of the resonant frequency by the frequency differencing technique previously described, and found $\omega/2\pi = (7.522 \pm 0.049)$ MHz. Using the relation $\omega = \gamma B_0$ at resonance, and measurements of B_0, we have calculated the gyromagnetic ratio in terms of the g-factor. We obtained $g = 5.58 \pm 0.03$.

4.2. Relaxation times vs. viscosity

We have performed T_1 and T_2 measurement for various glycerine-water mixtures, using the $90° - \tau - 90°$ and Carr-Purcell pulse sequences respectively. The degree of mixing (i.e. glycerine percent weight) was converted into a measure of viscosity via [7]. Figure 2 shows the typical growth of the secondary FID amplitude as a function of τ in the T_1 measurement. The results from various τ have been superimposed in order to illustrate the exponential characteristic of the spin-lattice relaxation.

To each of the secondary FIDs, we were able to fit a decaying sinusoid. We then extrapolated the exponential envelope to the beginning of the FID. The initial amplitude was taken to be the "height" of the secondary FID. As shown in Figure 2, the exponential model was an excellent characterization of the relaxation process. This analysis was performed for each of the available mixtures, yielding T_1 values as function of viscosity.

For the spin-spin relaxation measurements, we have used a much simpler numerical procedure. This was necessary due to several factors: (1) the double-sided exponential envelope proved to be a more difficult function to fit numerically; and (2) the spin echoes from the Carr-Purcell sequences were embedded in long data vectors that were difficult to parse reliably. With this in mind, Figure 3 illustrates the procedure we have used to deduce T_2 from the Carr-Purcell response.

We began by considering two adjacent spin echoes (top panel), from which the basic period was deduced. Using

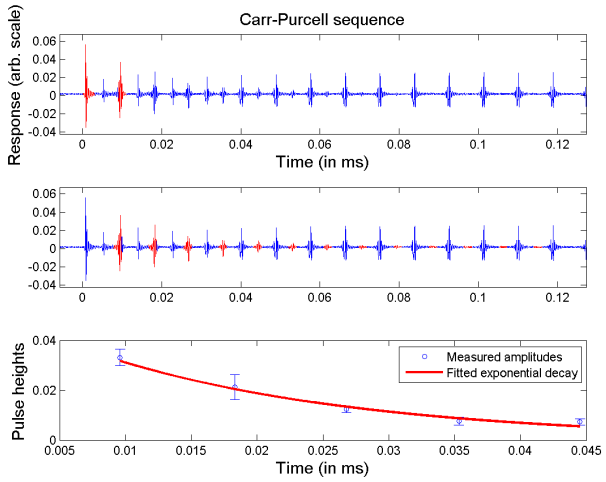

FIG. 3: Illustration of the Carr-Purcell analysis on 98% glycerine. The basic periodicity of the signal is deduced by considering the first two FIDs (top). Based on the computed period, the spin echoes are identified (middle). Finally, an exponential regression of the echo peaks is performed. Here, we obtain $T_2 = 20.0 \pm 2.2$ ms, and $\chi^2_{\nu-1} = 1.23$.

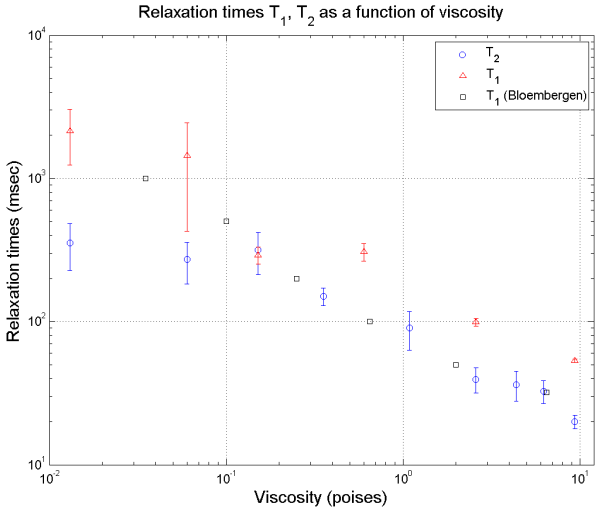

FIG. 4: Relaxation times T_1 and T_2 as a function of sample viscosity. Bloembergen's original data for T_1 is also plotted for comparison. We have verified Bloembergen's observation of the inverse relationship between T_1 and viscosity.

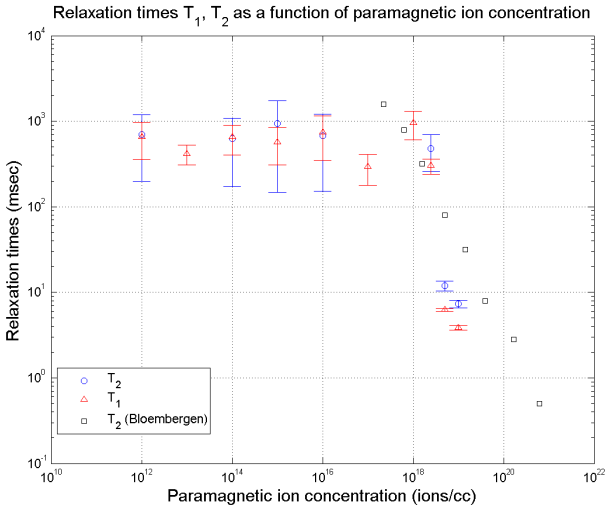

FIG. 5: Relaxation times T_1 and T_2 as a function of impurities. Bloembergen's original data for T_2 is also plotted for comparison. Note the threshold effect near 10^{17} ions/cc.

this spacing, we were able to grab each echo (middle). For each, we then computed the value of the maximum height (bottom). Note that this "peak sampling" technique for T_2 is more susceptible to aliasing issues than the regression procedure for T_1, since the latter method is sensitive to the internal phase of the oscillatory signal. We have chosen to employ an estimate for the error in the height determination (for T_2) that would compensate for the additional susceptibility. Namely, we consider N neighboring points about the maximum, and use their standard deviation as the error. Note that if the sampled peak were not a true maximum in the original signal, we expect larger standard deviation in the set of neighborhood points, since the slope will be nonzero.

These procedures yielded T_1 and T_2 values as presented in Fig 4. For comparison, Bloembergen's original study of the viscosity dependence of T_1 is also plotted. It is evident that our measurements yield a slope parallel to Bloembergen's results. Hence, we confirmed Bloembergen's inverse-law observation between the relaxation times vs. viscosity. As we have predicted, additional microscopic interactions (a more viscous sample) increases the relaxation rates.

4.3. Relaxation times vs. paramagnetic ion doping

The above T_1 and T_2 fitting procedures were repeated on a sequence of samples that were doped with various Fe^{3+} concentrations. The addition of these ions are expected to increase relaxation rates, since they contribute to microscopic spin-spin interactions within the sample. The results are plotted in Fig. 5.

Unfortunately, only limited comparisons to Bloembergen's data can be made, because the available range of concentrations did not overlap well with Bloembergen's samples. However, in the overlapping regions, we have found plausible agreement with the original study. In addition, below 10^{17} ions/cc levels, we have observed an interesting saturation behavior of the relaxation times. There are many possible interpretations of this phenomenon. The plateau may reflect a threshold effect in the impurity concentration. It may also be the case that some imperfection within our apparatus placed a ceiling in the relaxation times at the 1s range. Or, in the worst case, it may signify flawed numerical procedures or defective samples. In general, however, the basic claim that

increased microscopic complexity leads to faster relaxation rates is supported by our measurements.

5. ERROR ANALYSIS

We have resorted to the "peak-sampling" technique for measuring heights of spin echoes due to its simplicity. Ideally, the pulses should be characterized by a full regression, as was performed for the T_1 analysis. The main advantage is that the latter procedure is sensitive to the internal phase of the oscillatory signal, and is therefore less susceptible to aliasing issues in the sampling process. In particular, we have performed both techniques on T_1 data, and have found up to 100ms discrepancies in the resulting relaxation times.

We remarked previously that an estimate of the peak error (due to aliasing) may be obtained by considering the neighborhood of the maximal point. Such errors were typically on the order of 0.005 (in the arbitrary units of the sampling process). This can be compared to the intrinsic digitization error of 0.0006 of our equipment. Hence, if the proper fittings are performed in the spin echoes, it is in principle possible to obtain a factor of ten reduction in the echo height errors.

More fundamentally, we have observed that the envelope of each FID and spin echoes are not perfect exponentials. Some of this deviation may be observed in the FID of Fig. 2 where the tail shows discrepancies in the expected amplitude, as well as the oscillation frequency. Thus, we suspect that our fitting functions $V(t) = \alpha e^{-\gamma t}\sin(\omega t + \phi) + \delta$ may be theoretically incomplete.

We have already discussed several instrumental shortcomings. In addition, we also believe that some of the paramagnetic ion samples may have been improperly prepared. For instance, precipitation was observed in many of the samples, which is clearly inappropriate for our experiment.

6. CONCLUSIONS

We have investigated relaxation phenomena in a sample of nuclear spins. The spin-lattice relaxation T_1 and the spin-spin relaxation T_2 times were measured as a function of sample viscosity and impurity concentrations. For the former, we have verified Bloembergen's observation that the relaxation times are inversely related to the sample viscosity. The study of impurity effects remains inconclusive. We require more samples in the range of Bloembergen's original study for a better assessment. In general, our experiment corroborates the intuition that additional microscopic interactions (increased viscosity, additional impurities) increases relaxation rates.

[1] N. Bloembergen, *Nuclear Magnetic Relaxation* (W.A. Benjamine, 1961).
[2] K. Lee and W. Anderson, *Nuclear spins, moments, and magnetic resonance frequencies* (CRC Press, 1967).
[3] C. Cohen-Tannoudji, B. Diu, and F. Laloe, *Quantum Mechanics* (Wiley-Interscience, 2006).
[4] J. lab staff, *Pulsed NMR lab guide* (2008).
[5] E. Hahn, Phys. Rev. (1950).
[6] S. Sewell, *Pulsed Nuclear Magnetic Resonance* (MIT Copy Tech, 2005).
[7] *Viscosity of aqueous glycerine solutions*, http://www.dow.com/glycerine/resources/table18.htm.

Acknowledgments

As usual, THK gratefully acknowledges Connor McEntee for his partnership in the experiment.